JOURNAL OF MORPHOLOGY 271:293–304 (2010)

Ultrastructure of Spermiogenesis in the Cottonmouth, *Agkistrodon piscivorus* (Squamata: Viperidae: Crotalinae)

Kevin M. Gribbins,[1]* Justin L. Rheubert,[1,2] Marla L. Anzalone,[1] Dustin S. Siegel,[3] and David M. Sever[2]

[1]*Department of Biology, Wittenberg University, Springfield, Ohio 45501*
[2]*Department of Biological Sciences, Southeastern Louisiana University, Hammond, Louisiana 70402*
[3]*Department of Biology, Saint Louis University, St. Louis, Missouri 63103*

ABSTRACT To date multiple studies exist that examine the morphology of spermatozoa. However, there are limited numbers of data detailing the ontogenic characters of spermiogenesis within squamates. Testicular tissues were collected from Cottonmouths (*Agkistrodon piscivorus*) and tissues from spermiogenically active months were analyzed ultrastructurally to detail the cellular changes that occur during spermiogenesis. The major events of spermiogenesis (acrosome formation, nuclear elongation/DNA condensation, and flagellar development) resemble that of other squamates; however, specific ultrastructural differences can be observed between Cottonmouths and other squamates studied to date. During acrosome formation vesicles from the Golgi apparatus fuse at the apical surface of the nuclear membrane prior to making nuclear contact. At this stage, the acrosome granule can be observed in a centralized location within the vesicle. As elongation commences the acrosome complex becomes highly compartmentalized and migrates laterally along the nucleus. Parallel and circum-cylindrical microtubules (components of the manchette) are observed with parallel microtubules outnumbering the circum-cylindrical microtubules. Flagella, displaying the conserved 9 + 2 microtubule arrangement, sit in nuclear fossae that have electron lucent shoulders juxtaposed on either side of the spermatids basal plates. This study aims to provide developmental characters for squamates in the subfamily Crotalinae, family Viperidae, which may be useful for histopathological studies on spermatogenesis in semi-aquatic species exposed to pesticides. Furthermore, these data in the near future may provide morphological characters for spermiogenesis that can be added to morphological data matrices that may be used in phylogenetic analyses. J. Morphol. 271:293–304, 2010. © 2009 Wiley-Liss, Inc.

KEY WORDS: spermiogenesis; ultrastructure; Cottonmouth; germ cell development

INTRODUCTION

In the last decade, the ultrastructure of the spermatozoa of Squamata has received much attention as far as its use in phylogenetic analyses. These studies have focused on aspects that may be useful for phylogenetic inference because gamete ultrastructure has been considered a rich source of nontraditional characters (Jamieson, 1991; Newton and Trauth, 1992; Jamieson et al., 1995; Teixeira et al., 1999; Tavares-Bastos et al., 2002; Vieira et al., 2004, Wiens 2004). Nevertheless, descriptions of spermatozoa ultrastructure in snakes are limited at best (see Cunha et al., 2008 for review), and complete descriptions of the entire process of spermiogenesis within squamates are almost nonexistent (Gribbins et al., 2007). There are a number of studies that focus on specific parts of spermiogenesis (Hondo et al., 1994; Jamieson et al., 1996; Al-Dokhi, 2004; Al-Dokhi et al., 2004, 2006), but to our knowledge the only comprehensive spermiogenic study in squamates that covers acrosome development, flagellar formation, elongation, and condensation of the spermatid DNA was completed for the Ground Skink (*Scincella lateralis*) (Gribbins et al., 2007). Furthermore, within snakes, no data exist that detail the complete ultrastructure of spermiogenesis, and only two recent studies exist that details the ultrastructure of spermatozoa within the subfamily Crotalinae of Viperidae (Cunha et al., 2008; Tourmente et al., 2008).

The events of spermiogenesis should parallel the mature structures observed within functional spermatozoa. For example, a more stout, thicker nuclear head on mature spermatozoa may be linked to the reduction or complete lack of the manchette or a component of the manchette, which has been suggested for the Ground Skink (Gribbins et al., 2007). Spermiogenesis also provides the potential to identify more characters that could be used in combinations with those known for mature spermatozoa to increase the robustness of a phylogenetic matrix (Wiens, 2004). Understanding the process of spermiogenesis at the ultrastructural level

*Correspondence to: Kevin M. Gribbins, Department of Biology, Wittenberg University, PO Box 720, Springfield, OH 45501-0720. E-mail: kgribbins@wittenberg.edu

Received 28 May 2009; Revised 14 July 2009; Accepted 16 August 2009

Published online 13 October 2009 in Wiley InterScience (www.interscience.wiley.com)
DOI: 10.1002/jmor.10798

© 2009 WILEY-LISS, INC.

also provides valuable insight into the developmental process of sperm production and has the prospect of being a valuable histopathological tool in studies of how pesticides affect the process of spermatogenesis within amniotic testes. Indeed ultrastructural abnormalities have been identified in spermatogenesis, particularly during spermiogenesis, upon pesticide exposure in mammals (Russell et al., 1990).

The purpose of this study is to map the ultrastructural steps of spermiogenesis within the semiaquatic Cottonmouth, *Agkistrodon piscivorus*. This crotalid snake inhabits aquatic lowlands of the southeastern United States (Conant and Collins, 2001). They are often found in abundant numbers near permanent water sources within much of their geographic range, and are potentially a sentinel species for the histopathological study of how heavy metals and pesticides affect the testis and spermatogenesis. The spermatogenic cycle has been described previously, as well as a description of the germ cell development strategy during spermatogenesis at the level of the light microscope (Gribbins et al., 2008). The results of this study will be compared with the ultrastructure of spermatozoa of the South American Rattlesnake, *Crotalus durissus* (Cunha et al., 2008), *Bothrops alternatus* (Cross Pit Viper) and *diporus* (Bolivian Lancehead) (Tourmente et al., 2008), other squamates, and to the complete ultrastructural description of spermiogenesis in the Ground Skink, *Scincella lateralis* (Gribbins et al., 2007). Results from this study can subsequently be combined with ultrastructural data of spermiogenesis not only within snakes, but also within other squamates. With the future use of phylogenetic tools, the following data may aid in the understanding of how the spermiogenic process leads to the final morphology of mature spermatozoa and help resolve phylogenetic relationships within the squamate clade.

MATERIALS AND METHODS

Animal Collection

Adult male Cottonmouth snakes ($n = 8$), *Agkistrodon piscivorus,* were collected from southeastern Louisiana during the months of May, June, and September-November 2006, which are spermiogenically active months in Cottonmouths (Gribbins et al., 2008). Snakes were sacrificed using an intraperitoneal injection of sodium pentobarbital as approved by the Institutional Animal Care and Use Committee at Southeastern Louisiana University, and the testes were removed and fixed in Trump's fixative (EMS, Hatfield, PA). The testes were then cut into transverse sections and stored under refrigeration (4°C).

Tissue Preparation

Testicular tissues were dissected out and cut into 2–3 mm blocks and washed twice with cacodylate buffer (pH 7.0) for 20 min each. They were then post-fixed in 2% osmium tetroxide for 2 h, washed with cacodylate buffer (pH 7.0) three times for 20 min each, dehydrated in a graded series of ethanol solutions (70%, 85%, 95% X2, 100% X 2), and cleared with two 10 min treatments of propylene oxide. Each piece of testis was then gradually introduced to epoxy resin (Embed 812, EMS, Hatfield, PA) (2:1 and 1:1 solutions of 100% ethanol: epoxy resin). Tissues were then placed in pure Embed 812 for 24 h. Fresh resin was prepared and the tissues were embedded in small beam capsules, and subsequently cured for 48 h at 70°C in a Fisher isotemperature vacuum oven (Fisher Scientific, Pittsburg, PA). Sections (90 nm) were obtained by use of a diamond knife (DDK, Wilmington, DE) on an LKB automated ultramicrotome (LKB Produkter AB, Bromma, Sweden). Sections were then placed on copper grids and stained with uranyl acetate and lead citrate.

Ultrastructural Analysis

The samples were viewed using a Jeol JEM-1200EX II transmission electron microscope (Jeol). Micrographs were taken of representative spermatids and structural components associated with spermiogenesis via a Gatan 785 Erlangshen digital camera (Gatan, Warrendale, PA). The micrographs were then analyzed and composite plates were assembled using Adobe Photoshop CS (Adobe Systems, San Jose, CA).

RESULTS

Germ cells develop within the seminiferous tubules of the Cottonmouth testis. The spermatids, which undergo spermiogenesis, are located centrally within the germinal epithelium in association with the lumen of the seminiferous tubule (Fig. 1A, B). Once spermiogenesis is completed mature spermatozoa are shed to this lumen for transport to the excurrent duct system. The onset of spermiogenesis is highlighted by the accumulation of round spermatids within the seminiferous epithelium of *Agkistrodon piscivorus* immediately following meiosis. During these early stages, an acrosome vesicle (Fig. 2A, insert, white arrowhead) and a juxtapositioned Golgi apparatus (Fig. 2C, black arrow) dominate the spermatid cytoplasm near the apex of the nucleus. The acrosome vesicle does not make contact with the nuclear membrane (Fig. 2A, insert) and a small diffuse acrosome granule is centrally located within this vesicle. The cytoplasm is also packed with mitochondria (Fig. 2A, white arrow), multivesicular bodies, (Fig. 2A, black arrowhead) and endoplasmic reticula (Fig. 2A, black arrow).

Once contact is made between the acrosome and the nucleus, the acrosome vesicle begins to increase in size and a large prominent acrosome granule is observed (Fig. 2B, AV and D, white arrowhead). The granule sits in a basal position on the inner membrane of the acrosome vesicle. The vesicle and granule increase in size presumably from merging transport vesicles (Fig. 2C, white arrowhead) that originate from the most proximal cisternum of the Golgi complex (Fig. 2C. black arrow). As the acrosome complex increases in size, it causes the nuclear fossa to enlarge resulting in a large indentation on the apical nuclear membrane. A prominent subacrosome space is already

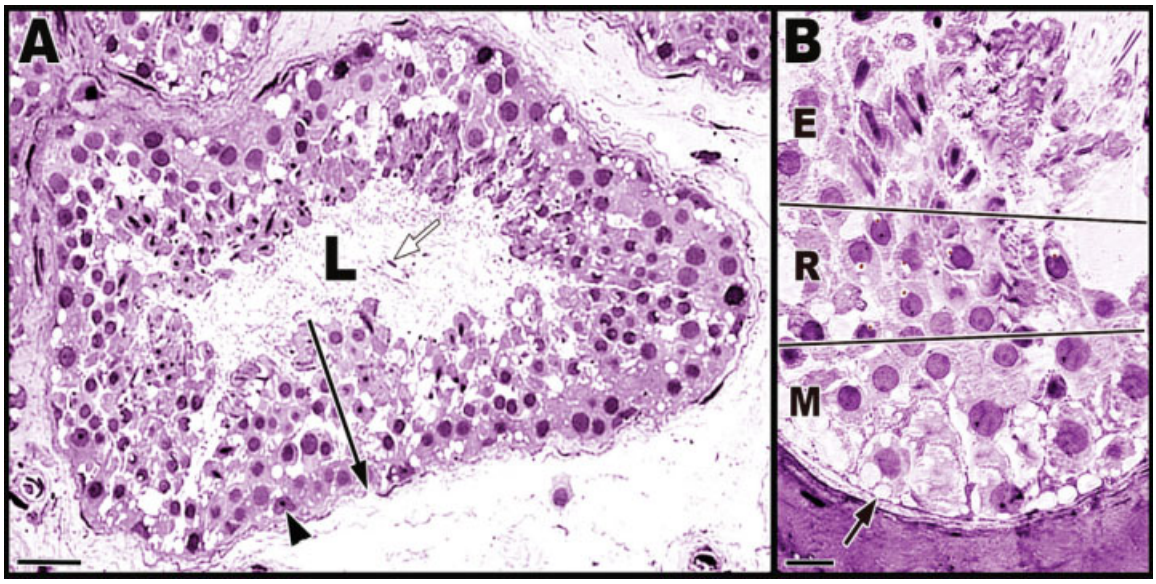

Fig. 1. Light microscope views of a June seminiferous tubule in the Cottonmouth testis. (A) Low power view of the seminiferous tubule in transverse section. The tubule has a wide Lumen (L) that is full of freshly spermiated spermatozoa (white arrow). The germinal epithelium is thick (black arrowhead) and contains developing germ cells and Sertoli cells (black arrowhead). Bar = 50 μm. (B) High power view of the germinal epithelium showing the generations of developing germ cells. The spermatogonia and spermatocytes (M) are located near the basement membrane (black arrow) at the periphery of the seminiferous tubule. The round spermatids (R), which are situated between the meiotic/mitotic cells and the elongating spermatids, show nice acrosomes with prominent acrosome granules. The elongating spermatids (E) are located near the apex of the germinal epithelium in close proximity to the lumen. Bar = 20 μm. [Color figure can be viewed in the online issue, which is available at www.interscience.wiley.com.]

forming during this early stage of development between the apical nuclear membrane and the inner acrosome vesicle membrane (Fig. 2C, white arrow). Within the subacrosome space, a dark band of electron dense protein can be visualized just superficial to the apical nuclear membrane (Fig. 2D, black arrow). Toward the climax of the round spermatid stage, the most distal part of the nucleus starts elongation. Near this site of elongation, the proximal centriole is observed in sagittal section and the elongating caudal neck region of the flagellum is also seen in transverse section (Fig. 2D, black arrowhead and white arrow). The distal neck demonstrates the conserved 9 + 2 microtubule arrangement (Fig. 2D insert) and the sagittal view of proximal centriole reveals the peripheral microtubules sagittally (Fig. 2D, insert). Also, note the enlarged peripheral fibers at microtubules 3 and 8 (Fig. 2D, insert, black arrow). During the early round stages of spermiogenesis the nucleus contains mostly diffuse euchromatin with only a few pockets of dense staining heterochromatin near the nuclear membrane.

As elongation continues, acrosome vesicle formation terminates, the vesicle begins to envelop the nucleus by moving caudally along its lateral edges, and the acrosome granule is seen as a centralized enlarged dark mass within the vesicle (Fig. 3A, white arrowhead). There is also flocculent material diffusing off of the granule and into the lumen of the acrosome vesicle (Fig. 3A, *). Chromatin condensation commences and the chromatin begins to condense in a spiral fashion (Fig. 3A insert) leaving pits of chromatin free areas within the nucleoplasm (Fig. 3D, white arrow). As the chromatin condenses the nucleus begins to stain more intensely. Flagellar elongation continues and the proximal and distal centrioles become more prominent (Fig. 3B, PC and DC). Two chromatin absent shoulders (Fig. 3B, C inserts) are found on the caudal portion of the nucleus located on either side of the nuclear fossa, which serves as the flagellar insertion point (Fig. 3C, black arrow). As the acrosome vesicle envelops the nucleus, the protein plaque becomes thicker within the subacrosome space (Fig. 3D, white arrowhead). Where the acrosome shoulders meet the nucleus, there is a raised flaring of the nuclear/acrosome membrane (Fig. 3D, black arrow). Dark condensing materials also can be seen accumulating just under the outer acrosome membrane during the climax of acrosome envelopment (Fig. 3D, black arrowhead).

During the peak of elongation, the acrosome vesicle envelops the entire nuclear apex (Fig. 4A, AV). The shoulders of the acrosome vesicle have migrated caudally and lay superficial to the apical nucleus. Just inside of the outer acrosome membrane is a continuous band of protein accumulation that spans the entire length of the acrosome vesicle (Fig. 4B, black arrow). The subacrosomal

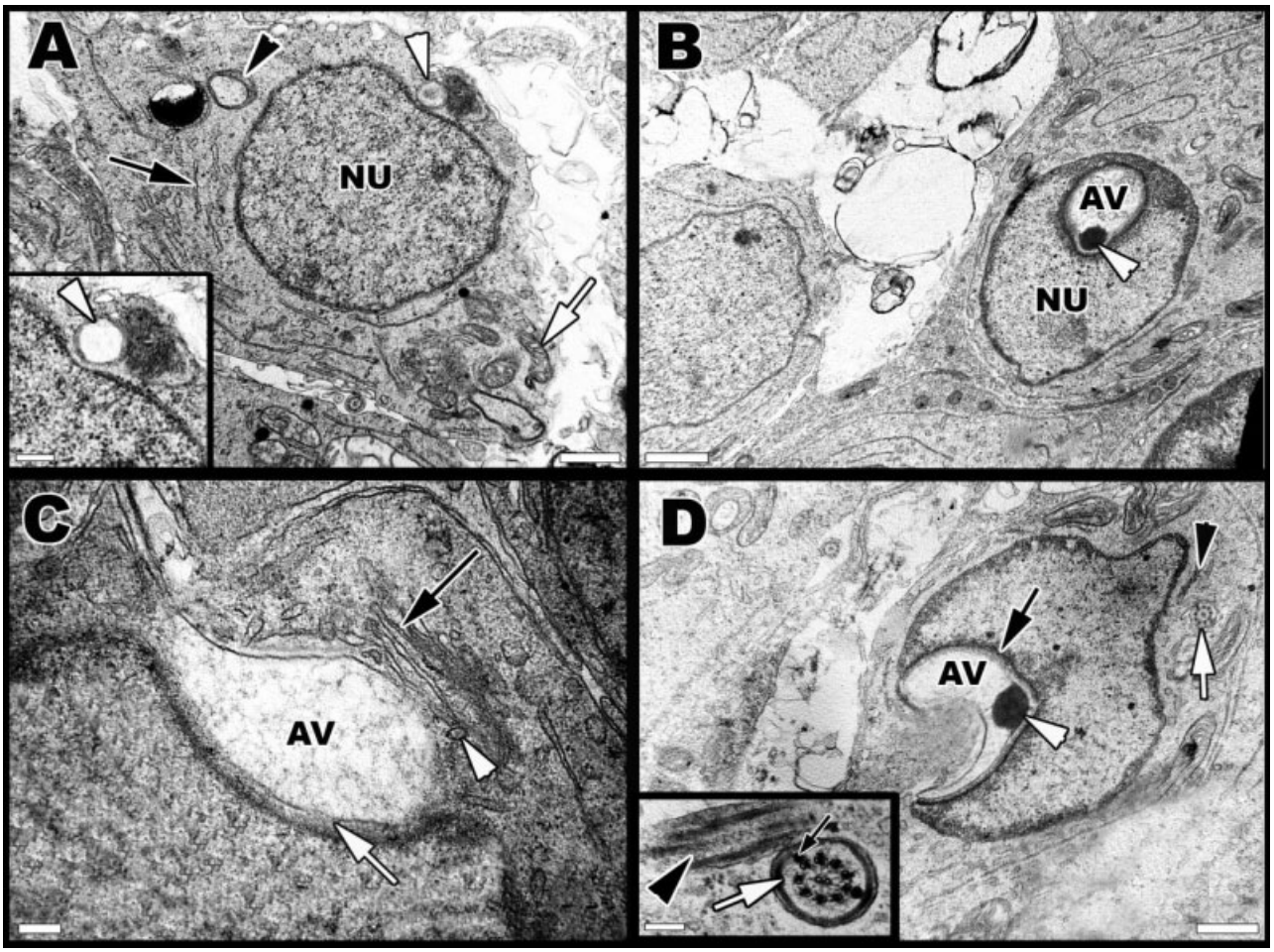

Fig. 2. Round spermatids undergoing acrosome development during the early stages of spermiogenesis within the seminiferous epithelium. (A) The acrosomal vesicle (white arrowhead) is juxtapositioned to the apical portion of the nucleus (NU). The vesicle is in the early phase of growth. The cytoplasm of the spermatid has numerous mitochondria (white arrow), many layers of endoplasmic reticula (black arrow), and multivesicular bodies (black arrowhead). Bar = 1 μm. Inset: Shows that the vesicle (white arrowhead) has not quite made contact with the nuclear membrane. Bar = 0.2 μm. (B) Transverse view of an acrosome later in development showing the attachment of the acrosomal vesicle (AV) to the apical portion of the nucleus (NU) and the presence of the acrosomal granule (white arrowhead). Bar = 1 μm. (C) The golgi apparatus (black arrow) is prominent and next to the developing acrosome (AV). Transport vesicles (white arrowhead) can be seen budding off of proximal cisterna of the golgi and presumably will merge with the acrosome during its growth phase. A prominent subacrosomal space (white arrow) is also developing between the acrosome membrane and the nuclear membrane. Bar = 0.2 μm. (D) Late stage round spermatid exhibiting a deep indented acrosome (AV) and a prominent acrosomal granule (white arrowhead). An accumulation of dark staining proteins is lining the nuclear membrane side of the subacrosomal space (black arrow). The caudal portion of the nucleus has begun elongation and the proximal centriole (black arrowhead) can be seen in sagittal section and the growing distal neck is shown in transverse section (white arrow) near the caudal end of the nucleus. Bar = 2 μm. The insert shows the proximal centriole (black arrowhead) and distal neck (white arrow) in greater detail. The developing neck of the flagellum has two opposing peripheral fibers (black arrow) associated with microtubule doublets 3 and 8. Bar = 0.2 μm.

space (Fig. 4B, *) is filled with a granulated protein plaque that sits on top of the round apical nipple of the nucleus. There are several Sertoli cell membranes that wrap around the acrosome complex (Fig. 4C, black arrowhead). Flagellar elongation continues and the number of mitochondria (Fig. 4D black arrow) surrounding the flagellum (Fig. 4D, white arrow) increases. Cytoplasmic droplets with lipid droplet cores (Fig. 4D, CD and LD) can often be visualized budding from developing spermatids, which will decrease the amount of cytoplasmic material associated with the nuclear head and developing midpiece.

During late elongation the chromatin becomes fully condensed and stains uniformly across the entire nucleus (Fig. 5, NU). The microtubules of the manchette (Fig. 5A and C, black arrows and black arrowheads) become evident on the lateral aspects of the nucleus as the spermatid continues to elongate. Both parallel (black arrow) and cir-

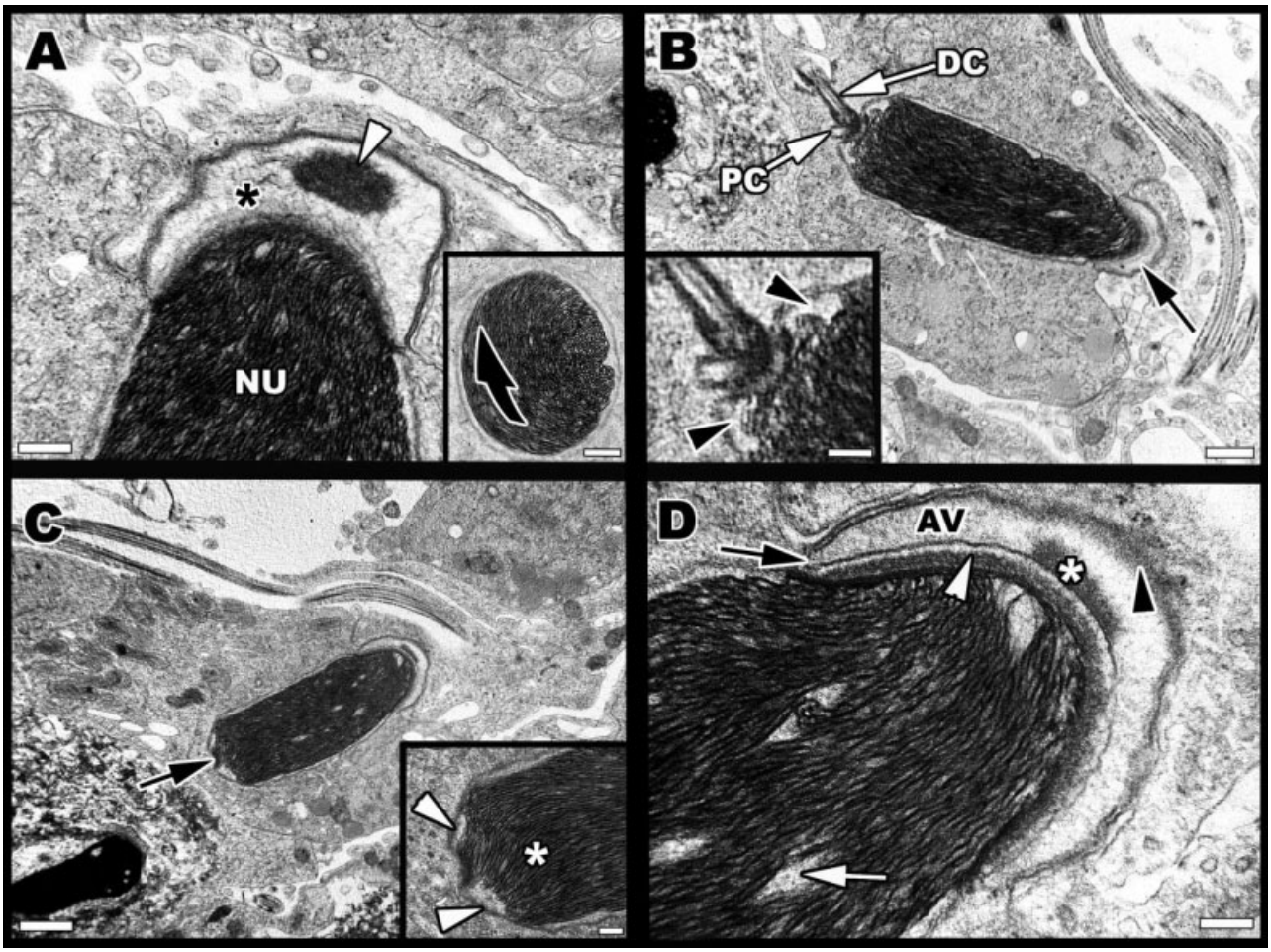

Fig. 3. The middle stage of spermatid elongation within the seminiferous epithelium. (A) The acrosome begins to flatten and envelop the elongating nucleus (NU) and the acrosomal granule (white arrowhead) migrates from its previous basal position within the vesicle to a more superficial location within the acrosome. The granule starts to break up and become diffuse within the acrosomal vesicle (*). Bar = 0.5 μm. The insert displays the same elongate step in transverse section and the arrow demonstrates the rotation of the chromatin as it condenses. Bar = 1 μm. (B) The developing flagellum is prominent in sagittal sections of elongates showing the presence of both the proximal (PC) and distal (DC) centrioles. The distal centriole begins to elongate to form the neck. On the opposite pole of the elongate is the acrosome vesicle (black arrow). Bar = 1 μm. The insert shows the two shoulders (black arrowheads), which are devoid of chromatin and can be seen lateral to the insert of the flagellum within the flagellar fossa. Bar = 0.2 μm. (C) Sagittal view of an elongate exhibiting the lateral shoulders (white arrowheads; insert) on the caudal portion of the nucleus and the flagellar fossa, which contains the basal plate (black arrow) where the proximal and distal centrioles attach. The white asterisk labels the spiraling condensation of DNA. Bar = 1 μm; Inset Bar = 0.2 μm. (D) A high power view of the acrosome vesicle (AV) of a slightly later staged middle elongate. The chromatin within the apical nucleus shows spiraling and large open nulceoplasmic spaces (white arrow). The acrosome vesicle shoulders (black arrow) have extended further over the apex of the nucleus. The diffuse acrosome granule (white*) is perfusing within the vesicle (AV). Some of the dense protein material is accumulating underneath the outer acrosome membrane (black arrowhead). Dense protein plaques are also found within the subacrosome space (white arrowhead). Bar = 0.5 μm.

cum-cylindrical (black arrowhead) aligning microtubules can be found surrounding the length of the nucleus beginning just caudally to the shoulders of the acrosomal vesicle. The nucleus is reduced into a thin rostrum apically, which extends up into the acrosome complex (Fig. 5B). A protein absent space (epinuclear lucent zone) just rostral to the tip of the nucleus extends into the subacrosome space (Fig. 5B, black arrowhead). An area devoid of dark staining material (Fig. 5B, *) creates two strata of granulated proteins (Fig. 5B, 1, 2) within the subacrosomal space. The proximal centriole (Fig. 5D, *) connects at the caudal portion of the nucleus within the nuclear fossa that has developed during early elongation. The distal neck of the flagellum extends from the distal centriole and is devoid of the fibrous sheath (Fig. 5D, white arrow). The neck region (Fig. 5D, white arrow) contains the centrioles but lacks an electrodense collar (neck cylinder) and pericentriolar material. The flagellum continues to elongate caudally and becomes surrounded by a surplus of fibrous blocks (Fig. 5D,

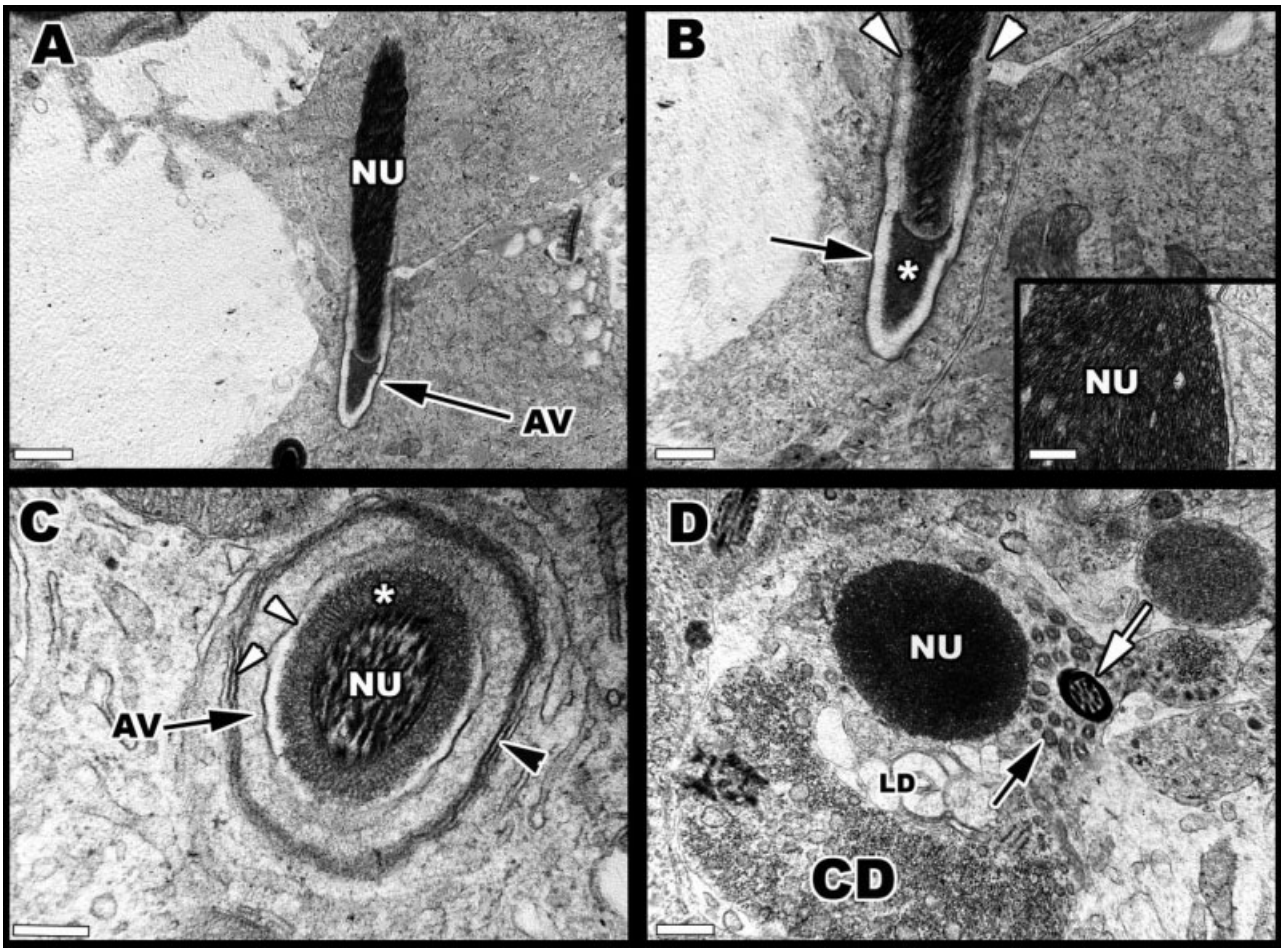

Fig. 4. An elongating spermatid nearing the climax of elongation. (A) The acrosomal vesicle (AV) envelops the entire nuclear (NU) apex. Bar = 1 μm. (B) The acrosomal shoulders (white arrowheads) are found 1/3 of the way down the lateral aspect of the nucleus. There is a very thin line of dark protein accumulation just deep to the outer acrosomal membrane (black arrow). The subacrosomal space (*) can be visualized separating the nucleus (NU) and the acrosome on the rostral portion of the developing spermatid and appears to be made up of large granular proteins. Bar = 1 μm. The insert shows further spiraling condensation of the chromatin and the nuclear spaces have been reduced significantly. Bar = 0.2 μm. (C) A cross-sectional view of the apical portion of a late elongate showing the acrosomal vesicle (AV) surrounding the nucleus (NU) with the subacrosomal space (*) separating the nucleus from the vesicle. The subacrosomal space is occupied by a dense layer of granulated proteins (*) and the inner and outer acrosomal membranes are easily visualized (white arrowheads). Several layers of Sertoli cell membrane encircle the outer acrosomal membrane (black arrowhead). Bar = 0.2 μm. (D) A cross-sectional view of the caudal portion of a late elongating spermatid nucleus (NU). The principal piece of the flagellum (white arrow) is seen in cross section near the nucleus and numerous mitochondria (black arrow) are accumulating between the nucleus and the flagellum. There is a large accumulation of degrading cytoplasm (CD) with a lipid droplet core (LD). Bar = 0.5 μm.

white arrowhead) creating a fibrous sheath around the midpiece and principal piece of the flagellum. During this stage, numerous elongated mitochondria (Fig. 5D, black arrow) start to accumulate just caudal to the neck, where the midpiece will be located in the mature spermatozoa.

The final stages of spermiogenesis demonstrate many of the structures present in the spermatid prior to being transferred to the lumina of the seminiferous tubules as mature spermatozoa during spermiation. The acrosome becomes cylindrical in shape (Fig. 6A) and surrounds the subacrosome space (Fig. 6B, white *) and a thin nuclear rostrum extends into the subacrosome space (Fig. 6A,D). Multilaminar layers of Sertoli cell membrane are common around the acrosome complex of these late developing spermatids (Fig. 6C, white arrow and D, white arrowhead). Where the acrosome shoulders meet the nucleus caudally, there are dense staining protein flanges (Fig. 6A, white arrow). A small band of electron dense protein material surrounds the inside of the entire outer membrane of the acrosome near its apex (Fig. 6B, white arrowhead). However, as you move caudally along the acrosome the band of protein is also seen just outside the outer acrosome membrane

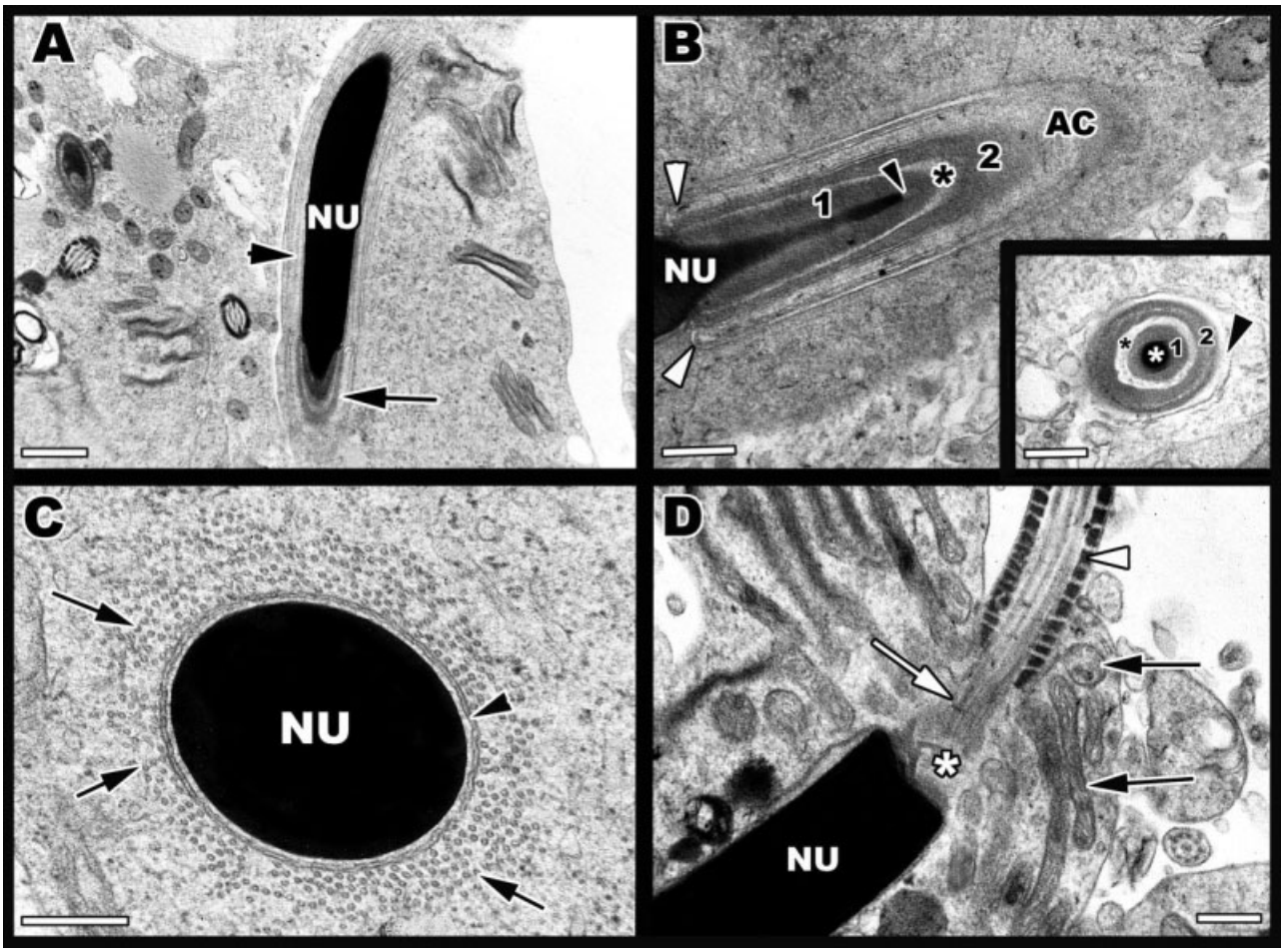

Fig. 5. A late elongate that has completed elongation and is finishing condensation of its DNA. (A) The chromatin of the nucleus (NU) lacks open pockets of nucleoplasm and the condensed DNA is uniformly stained. The microtubules composing the manchette (black arrowhead) can be seen in juxtaposition to the sagittally sectioned nucleus. The acrosome complex (black arrow) drapes over the apex of the nucleus, causing a conical shaped cranial nuclear head. Bar = 1 μm. (B) A high power view of the acrosome (AC) and the apical nucleus (NU). The acrosome shoulders (white arrowheads) are located where the elongation of the nuclear rostrum (thin nuclear process that extends into the acrosome complex) begins. The rostrum extends into the subacrosomal space and just beyond its tapered tip is a short epilucent zone (black arrowhead) that will eventually precede the more rostrally located perforatorium in terminating stages of spermiogenesis. The subacrosomal space is separated into two granulated protein layers (1 and 2) by a clear zone (*). Bar = 0.2 μm. The insert shows the acrosomal complex in transverse section near the tip of the nuclear rostrum (white *). This view confirms the two granulated protein layers (1 and 2) separated by a clear zone (black *) within the subacrosomal space. The acrosome vesicle is also seen in cross section (black arrowhead). Bar = 0.2 μm. (C) A transverse section through the body of the nucleus (NU) showing the uniformly stained DNA and the parallel microtubules of the manchette (black arrows) in cross-section. Also note that there is a small group of circum-cylindrical microtubules making up the inner most ring of the manchette (black arrowhead). Bar = 1 μm. (D) The caudal nucleus (NU) is also uniformly stained with condensed chromatin and the proximal centriole (white*) can be seen in cross-section juxtaposition to the distal centriole, which extends to form the neck (white arrow) of the flagellum. The principal piece/midpiece is easily distinguished from the neck by the thick ribs of the fibrous sheath (white arrowhead) that surrounds the microtubules of the flagellum. Mitochondria both in sagittal and transverse section (black arrows) are accumulating near what will be the midpiece of the mature spermatozoon. Bar = 0.2 μm.

(Fig. 6C, black arrowhead). The perforatorium (Fig. 6C, white arrowhead) extends through the most rostral region of the subacrosome space (Fig 6A,C, white arrowhead). The nucleus is uniformly stained and the chromatin has become fully condensed. The microtubules of the manchette can be visualized in both transverse and cross-sections of the late elongating spermatids (Fig 6A black arrow, E, black *). Most of the manchette microtubules are associated with the body of the nucleus below the acrosome and run its entire length (Fig. 6A, black arrow).

Dense enlarged peripheral fibers are associated with microtubules 3 and 8 within the caudal neck and midpiece portions of the axoneme (Fig. 6F, white arrow). Little to no pericentriolar material is associated with the proximal portions of the neck region/distal centriole. The midpiece has an

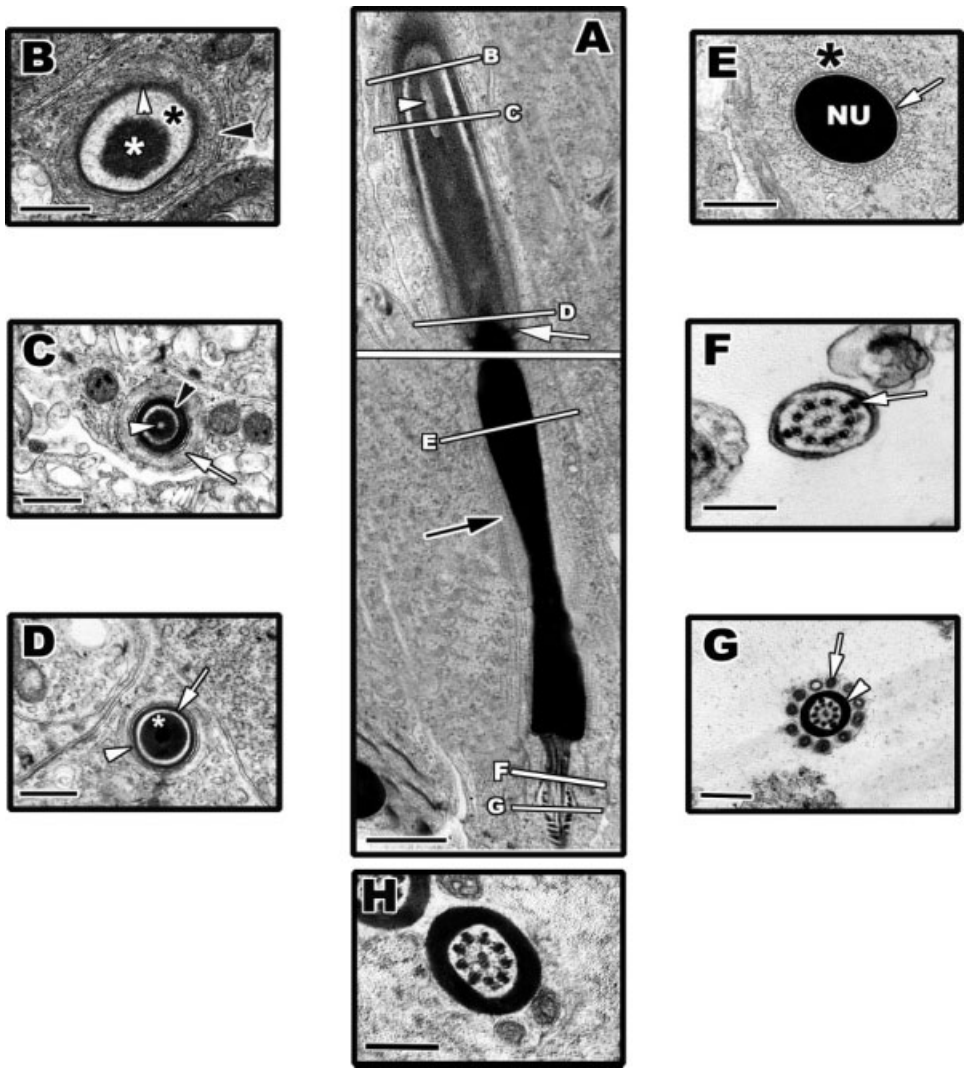

Fig. 6. (A) Sagittal section of an elongate at the end of spermiogenesis with all three major parts of the spermatid visible (acrosome, nucleus, and flagellum; the white line through the middle of (A) denotes that two separate micrographs were combined to obtain this image). Lines and represented letters show approximately where transverse sections (CS) occurred within spermatids at or near the same stage of development as (A) in order to obtain cross-sections B–G. Note the well-developed parallel microtubules of the manchette (black arrow) running alongside the nucleus, the perforatorium (white arrowhead), and the dark staining flange associated with the acrosome shoulders and the nucleus (white arrow). Bars = 2 μm. (B) CS through the *rostral* subacrosomal space and acrosomal vesicle. Granulated protein layer of subacrosomal space (white*), acrosomal vesicle (black*), protein accumulation on the inside of the outer acrosomal membrane (white arrowhead), multiple Sertoli cell membranes surrounding the acrosome vesicle (black arrowhead). (C) CS through the subacrosomal space, perforatorium, and acrosomal vesicle. The white arrowhead points to the perforatorium, which is surrounded by the granulated proteins of the subacrosomal space. The white circular region around the subacrosomal space is the acrosomal vesicle, which again has protein accumulations under its outer membrane (black arrowhead). Also note the numerous Sertoli cell membrane layers surrounding the entire acrosomal complex (white arrow). (D) CS through the nuclear rostrum. The white * labels the subacrosomal space. Within the middle of this space is the conical point of the rostrum in CS. Also present are the protein accumulation under the outer membrane of the acrosome (white arrow) and the Sertoli cell membrane layers (white arrowhead). (E) CS through the nucleus proper. Nucleus (NU), Manchette (*), inner single circum-cylindrical microtubule layer (white arrow). (F) CS through the distal neck of the flagellum. Axoneme is nicely represented with nine outer pairs of microtubules and a single central microtubule doublet, indicating that the section represents the beginning of the elongating flagellum and is most likely the transition point between the distal centriole and the midpiece. Attached enlarged peripheral fibers (white arrow) are seen at microtubule doublets three and eight within the axoneme. (G) CS through the midpiece. Dense fibrous sheath/ring (white arrowhead), concentric mitochondria (white arrow). (H) A transverse section of the principle piece that represents the majority of the flagellum caudal to the midpiece. Note there are no enlarged peripheral fibers associated with the axoneme below the midpiece. Bar = 0.2 μm for all CS.

axoneme that is surrounded by mitochondria with no dense bodies found associated with these mitochondria (Fig. 6G, white arrow). It qualitatively appears that 11 mitochondria normally surround the distal centriole in transverse sections through the midpieces of late elongating spermatids. The principle piece (Fig. 6H) has a thick fibrous sheath around it below the midpiece up to the end piece (not shown in Fig. 6). There are no or very reduced peripheral fibers associated with microtubule doublets 3 and 8 within the principle piece axoneme.

DISCUSSION

Ultrastructural analysis of spermiogenesis within *Agkistrodon piscivorus* reveals many characters that are common among Squamata and ophidians and some characters that may be unique to *A. piscivorus* and/or the *Agkistrodon* complex. Throughout spermiogenesis three major events occur that lead to mature spermatozoa: acrosome formation, DNA condensation/nuclear elongation, and flagellar development. During these stages of maturation, the characters found within mature spermatozoa become visible and can be described in a developmental fashion.

During acrosome formation in *Agkistrodon piscivorus* the acrosome vesicle forms from transport vesicles budding from the Golgi apparatus, which accumulate as an intact acrosome vesicle before contact is made with the nuclear membrane. This is similar to what has been described in *Scincella lateralis* (Ground Skink) (Gribbins et al., 2007). Also, the acrosome granule is seen within this vesicle before nuclear contact, but in contrast to the basal positioned granule described in *S. lateralis*, the granule is centrally located and then migrates to its basal position once the acrosome makes contact with the nucleus. The granule makes its largest growth spurt in this basal position within the acrosome of *A. piscivorus*. During nuclear contact between the vesicle and the nuclear membrane, an indentation where the acrosome is seated can be visualized in the nucleus and is a characteristic of spermiogenesis in vertebrates. Subsequent features of acrosome development within *A. piscivorus* are similar to that described for *S. lateralis* and other squamates such as: transport vesicles from the Golgi, prominent subacrosomal space, multilaminar Sertoli cell membranes, and lateral folding (Clark, 1967; Da Cruz-Landim and Da Druz-Hofling, 1977; Butler and Gabri, 1984; Dehlawi et al., 1992, Ferreira and Dolder, 2002, 2003; Gribbins et al., 2007).

As early elongation begins in *Agkistrodon piscivorus*, it becomes apparent that the acrosome complex is highly compartmentalized, which is common in most squamates (Healy and Jamieson, 1994; Harding et al., 1995; Jamieson and Scheltinga, 1994; Jamieson et al., 1996; Tavares et al., 2007). This complex compartmentalization has been suggested to aid in the release of hydrolytic enzymes that penetrate the outer layers of the ovum during fertilization (Talbot, 1991). The compartments include the subacrosomal space, perforatorium, acrosomal vesicle, and the outer Sertoli cell membrane layers, which are all similar to other squamates including the Ground Skink (Gribbins et al., 2007); however, stratification occurs to the subacrosome space and an epinuclear lucent area is present within *A. piscivorus* spermatids. In some squamates, such as *Iguana iguana,* portions of the acrosome have originated from the endoplasmic reticulum (Ferreira and Dolder, 2002); however, there is no evidence of endoplasmic reticulum participation in *A. piscivorus* spermatids or *Scincella lateralis* spermatids.

The acrosome granule formation is described for other squamates and mammalian species as the accumulation of proacrosomal granules (Russell et al., 1990), which in lizards (except *Scincella lateralis*) occurs when the acrosome contacts the nuclear membrane (Del Conte, 1976; Gribbins et al., 2007). In both *S. lateralis* and *Agkistrodon piscivorus* the acrosome granule can be observed prior to the acrosome vesicle making contact with the nuclear membrane, which may suggest this trait is a potential synapomorphy for scleroglossids. This acrosome granule is responsible for the formation of the perforatorium, which is present in all squamates studied to date, including *A. piscivorus* (Ferreira and Dolder, 2002; Gribbins et al., 2007; Cunha et al., 2008).

During elongation in *Agkistrodon piscivorus* the nuclei are displaced apically within the cytoplasm and come in contact with the cell membranes of the developing spermatids as described in *Scincella lateralis* (Gribbins et al., 2007). This peripheral location of the spermatid nucleus has been hypothesized to be the cause of acrosome collapse and migration laterally (Clark, 1967; Butler and Gabri, 1984), the relocation of cellular organelles (Sprando and Russell, 1988; Soley, 1997; Lin and Jones, 1993, 2000; Ventela et al., 2003), and may aid in the removal of cytoplasmic fluid.

Nuclear elongation and DNA condensation occurs throughout the majority of late spermiogenesis. During this stage, the manchette can be visualized in both transverse and sagittal sections in Cottonmouth spermatids and has been hypothesized to aid in the elongation of the nucleus (Russell et al., 1990). Parallel microtubules outnumber the circum-cylindrical fibers in *Agkistrodon piscivorus*. This absence or limited numbers of circum-cylindrical microtubules is also noted in *Scincella lateralis* (Gribbins et al., 2007), which have thicker more robust bodied spermatozoa than that of other squamate species (Jamieson and Scheltinga, 1994). The result of fewer circum-cylindrical fibers may also result in more robust spermatozoa in *A. piscivorus*,

because the presence of circum-cylindrical fibers are thought to aid in thinning out the width of the nucleus during elongation. During DNA condensation, the chromosomes condense in a spiral fashion, which was not reported in *S. lateralis* but was noted by Ferreira and Dolder (2003) in the lizard *Tropidurus itambre*, and by Al-Dokhi (2004) in the snake *Cerastes cerastes,* resulting in large areas of open nucleoplasm. Also, during the condensation of nuclear material, uniform translucent areas are observed on either side of the caudally located nuclear fossa where the flagellum attaches to the nuclear body of the developing spermatid. These lucent structures have not been described in any other reptile during spermiogenesis and thus far appear unique to *A. piscivorus*. This developmental novelty may be an autapomorphic character during spermiogenesis for *A. piscivorus* or possibly a synapomorphy for the *Agkistrodon* complex if this character is only observed in congeners of *A. piscivorus*. However, too few squamates have been investigated to accurately assess character polarity of spermiogenesis in this taxon.

As flagellar development continues large numbers of mitochondria become present in the posterior portion of the *Agkistrodon piscivorus* spermatid cytoplasm and are associated with the flagellum, which is consistent with other amniotes (McIntosh and Porter, 1967; Lin and Jones, 1993; Ferreira and Dolder, 2002, Gribbins et al., 2007; Cunha et al., 2008). The axoneme of the distal neck, midpiece, and principal piece all display the conserved 9 + 2 microtubule arrangement seen in most amniotes. The previously described enlarged peripheral fibers located near microtubule doublets 3 and 8 (Healy and Jamieson, 1994; Ferreira and Dolder, 2003; Cunha et al., 2008; Tourmente et al., 2008) are considered a synapomorphy for Lepdiosauria (Sphenodonta + Squamata) and are also seen within the neck and midpiece axonemes of the flagella of *A. piscivorus.*

The processes of spermiogenesis in *Agkistrodon piscivorus* are very similar in most respects to other ophidians, which have limited data historically, and to other squamates studied to date. This suggests that many aspects of spermiogenesis are highly conserved within ophidian species and within Squamata. Also, much of the described data within this study corroborates the morphology of the mature spermatozoa described for the pitvipers *Crotalus durissus* (Cunha et al., 2008) and *Bothrops alternatus* and *diporus* (Tourmente et al., 2008). Presently, these two studies represent the only morphological data for spermatozoa or spermiogenesis within Crotalinae. Caution should be taken in making direct comparisons between the morphology of the mature spermatozoa and spermatids undergoing spermiogenesis as morphological modifications can occur post spermiogenesis to the spermatozoa as it passes through the excurrent duct system. Nevertheless, there are several noteworthy similarities and differences when comparing the spermatozoa of *Crotalus* and *Bothrops* with the spermatids of *A. piscivorus*.

The similarities that can be drawn from spermiogenesis in *A. piscivorus* compared with the spermatozoa of previously studied crotalids include the following. There is a more electron dense cortex and a lighter staining medulla to the acrosome of the mature spermatozoa of *Bothrops* and *Crotalus*. It can be hypothesized that the dark staining granular material just under the outer acrosome membrane of the Cottonmouth late elongating spermatid matures into the more electron dense cortex seen in the other crotalids. There is also a perforatorium rostrally located within the subacrosome space and an epinuclear lucent zone associated with the tip of the nucleus of Cottonmouth elongates similar to that found in the crotalid spermatozoa. The dark staining protein flange at the base of the acrosome shoulders in Cottonmouths is located in a similar place to the posterolateral flanges in the spermatozoa of *Bothrops*. Multilaminar membranes are associated with the outside of the acrosome and rostral nuclear head in Cottonmouth spermatids and *Crotalus* spermatozoa. Lastly, the neck and midpiece axonemes have enlarged peripheral fibers associated with microtubule doublets 3 and 8 in both Cottonmouths spermatids and the spermatozoa of the previously studied crotalids.

Differences are also observed between *A. piscivorus* spermiogenesis and the spermatozoa of *Crotalus durissus* and *Bothrops alternatus* and *disporus*. The stratification of the subacrosome space seen at the end of spermiogenesis in *A. piscivorus* is not present in the mature spermatozoa of *Crotalus* or *Bothrops*. Also, no annulus is present in late developing spermatids of *A. piscivorus*, which is present in the mature spermatozoa of crotalid spermatozoa. During spermiogenesis in *A. piscivorus* the development of dense bodies within the midpiece are not seen and there is no prominent dense collar or pericentriolar material around the neck of the elongating spermatids as seen in *C. durissus* spermatozoa. The translucent nuclear shoulders on either side of the flagellar insertion on the caudal end of elongating spermatids in Cottonmouths are not seen in the mature spermatozoa of *Crotalus* and *Bothrops*. The physiological, morphological, and evolutionary significance of these differences are unknown as comparative data is very sparse for ophidians within Viperidae. Furthermore, a companion study that includes the ultrastructural morphology of the spermatozoa of *A. piscivorus* must be completed so that direct comparison can be made between what is seen in spermiogenesis and the actual mature spermatozoa morphology in the recently studied crotalid species.

The analysis of spermiogenesis within the testes of *Agkistrodon piscivorus* is only the second complete morphological description of the entire spermiogenic cycle of a squamate (Gribbins et al., 2007). Although development of spermatozoa in Squamata appears conserved in many aspects, morphological differences are observed, and combining data from spermiogenesis and spermatozoa morphology may provide insight into the evolutionary relationships of squamates, and possibly the Amniota. Unfortunately to date, few data are available to reconstruct a firm understanding of spermiogenesis in reptiles, especially in a robust evolutionary context. Future data within Squamata, specifically Viperidae and Crotalinae, may help provide these details. This study, however, does provide solid morphological data on the developmental features of spermatid formation and provides baseline ultrastructural information for future histopathological studies regarding spermatogenesis within semi-aquatic Cottonmouths.

ACKNOWLEDGMENTS

The authors would like to thank Caleb D. McMahan for his useful insight on an earlier version of this manuscript. We would also like to thank Wittenberg University Summer Research Grants and The National Science Foundation (DEB-0809831) for funding this project.

LITERATURE CITED

Al-Dokhi OA. 2004. Electron microscopic study of sperm head differentiation in the Arabian Horned Viper *Cerastes cerastes (Squamata. Reptilia)*. J Biol Sci 2:111–116.

Al-Dokhi OA. 2006. Ultrastructure of sperm head differentiation in the lizard *Acanthodactylus boskinus (Squamata. Reptilia)*. J Zoolog Res 1:60–72.

Al-Dokhi OA, Al-Onazee YZ, Mubarak M. 2004. Light and electron microscopy of the testicular tissue of the snake *Eryx jayakari (Squamata. Reptilia)* with a reference to the dividing germ cells. J Biol Sci 3:345–351.

Butler RD, Gabri MS. 1984. Structure and development of the sperm head in the lizard *Podarcis (Lacerta) taurica*. J Ultrastructure Res 88:261–274.

Clark AQ. 1967. Some aspects of spermiogenesis in a lizard. Am J Anat 121:369–400.

Conant R, Collins JT. 2001. Reptiles and Amphibians, Eastern/Central North America. MA: Houghton Mifflin Company. pp 450.

Cunha LD, Tavares-Bastos L, Báo SN. 2008. Ultrastructural description and cytochemical study of the spermatozoon of *Crotalus durissus (Squamata. Serpentes)*. Micron 39:915–925.

Da Cruz-Landim C, Da Cruz-Hofling MA. 1977. Electron microscope study of lizard spermiogenesis in *Tropidurus torquatus* (*Lacertilia*). Caryologia 30:151–162.

Dehlawi GY, Ismail MF, Hamdi SA, Jamjoom MB. 1992. Ultrastructure of spermiogenesis of a Saudian reptile. The sperm head differentiation in *Agama adramitana*.. Arch Androl 28:223–234.

Del Conte E. 1976. The subacrosomal granule and its evolution during spermiogenesis in a lizard. Cell and Tissue Res 171:483–498.

Ferreira A, Dolder H. 2002. Ultrastructural analysis of spermiogenesis in *Iguana iguana (Reptilia: Sauria: Iguanidae)*. Eur J Morphol 40:89–99.

Ferreira A, Dolder H. 2003. Sperm ultrastructure and spermatogenesis in the lizard, *Tropidurus itambre*. Biocell 27:353–362.

Gribbins KM, Mills EM, Sever DM. 2007. Ultrastructural examination of spermiogenesis within the testis of the Ground Skink. Scincella laterale (Squamata, Sauria, Scincidae). J Morphol 268:181–192.

Gribbins KM, Rheubert JL, Siegel DS, Sever DM. 2008. Histological analysis of spermatogenesis and the germ cell development strategy within the testis of the male Western Cottonmouth Snake, *Agkistrodon piscivorus leucostoma*. Ann Anat 190:461–476

Harding HR, Aplin KP, Mazur M. 1995. Ultrastructure of spermatozoa of Australian Blindsnakes, *Ramphotyphlops spp*. (Typhlopidae, Squamata): First observations on the mature spermatozoon of scolecophidian snakes. In: Jamieson,BGM, Ausio J, Justine JL, editors. Advances in spermatozoal phylogeny and taxonomy. vol. 166. Mémoires du Musséum National d; Histoire Naturelle. pp 385–396.

Healy JM, Jamieson BGM. 1994. The ultrastructure of spermatogenesis and epididymal spermatozoa of the Tuatara *Sphenodon punctatus (Sphenodontidae. Amniota)*. Philosophical Transactions. Biolog Sci 344:187–199.

Hondo E, Kurohmaru M, Toriba M, Hayashi Y. 1994. Seasonal changes in spermatogenesis and ultrastructure of developing spermatids in the Japanese rat snake, *Elaphe climacophora*. J Vet Med Sci 56:836–840.

Jamieson BGM. 1991. Fish evolution and systematics: Evidence from spermatozoa. Cambridge, UK: Cambridge University Press.

Jamieson BGM. Ausio J, Justine JL. 1995. Advances in spermatozoal phylogeny and taxonomy. Mémoires du Musséum National d; Histoire Naturelle 166:1–565.

Jamieson BGM, Oliver SC, Scheltinga DM. 1996. The ultrastructure of the spermatozoa I. Scincidae, Gekkonidae, and Pygopididae (Reptilia). Acta Zool 77:85–100.

Jamieson BGM, Scheltinga DM. 1994. The ultrastructure of spermatozoa of the Australian skinks. Ctenotus taeniolatus, *Carlia pectoralis*, and *Tiliqua scincoides scincoides (Scincidae, Reptilia)*. Memoirs of the Queensland Museum 37:181–193.

Lin M, Jones RC. 1993. Spermiogenesis and spermiation in the Japanese quail (*Coturnix coturnix japonica*). J Anat 183:525–535.

Lin M, Jones RC. 2000. Spermiogenesis and spermiation in a monotreme mammal, the platypus, *Ornithorhynchus anatinius*. J Anat 196:217–232.

McIntosh JR, Porter KR. 1967. Microtubules in the spermatids of the domestic fowl. J Cell Bio 35:153–173.

Newton WD, Trauth SE. 1992. Ultrastructure of the spermatozoon of the lizard *Cnemidophorus sexlineatus (Sauria: Teiidae)*. Herpetologica 48:330–343.

Russell LD, Ettlin RA, Hikim AMP, Cleff ED. 1990. Histological and histopathological evaluation of the testis. Clearwater, FL: Cache River Press. pp 286.

Soley JT. 1997. Nuclear morphogenesis and the role of the manchette during spermiogenesis in the ostrich (*Struthio camelus*). J Anat 190:563–576.

Sprando RL, Russell LD. 1988. Spermiogenesis in the red-ear turtle (*Pseudemys scripta*) and the domestic fowl (*Gallus domesticus*): A study on cytoplasmic events including cell volume changes and cytoplasmic elimination. J Morphol 198:95–118.

Talbot P. 1991. Compartmentalization in the acrosome. In: Bacetti B, editor. Comparative spermatology-20 years after. New York: Raven Press. pp 255–259.

Tavares-Bastos L, Cunha LD, Colli GR, Báo SN. 2007. Ultrastructure of spermatozoa of scolecophidian snakes (Lepidosauria. Squamata). Acta Zool 88:189–197.

Tavares-Bastos L, Teixeira RD, Colli GR, Báo SN. 2002. Polymorphism in the sperm ultrastructure among four species of

lizards in the genus *Tupinambis (Squamata: Teiidae)*. Acta Zooloogica 80:47–59.

Teixeira RD, Vieira GHC, Colli GR, Bao SN. 1999. Ultrastructural study of spermatozoa of the neotropical lizards. Tropidurus semitaeniatus and *Tropidurus torquatus (Squamata, Tropiduridae)*. Tissue Cell 31:308–317.

Tourmente M, Giojalas L, Chiaraviglio M. 2008. Sperm ultrastructure of *Bothrops alternatus* and *Bothrops diporus* (Viperidae, Serpentes), and its possible relation to the reproductive features of the species. Zoomorphology 127, 241–248.

Ventela S, Toppari J, Parvinen M. 2003. Intercellular organelle traffic through cytoplasmic bridges in early spermatids of the rat: Mechanism of haploid gene product sharing. Mol Biol Cell 14:2768–2780.

Vieira GHC, Colli GR, Báo SN. 2004. The ultrastructure of the spermatozoon of the lizard Iguana iguana (Reptilia. Squamata, Iguanidae) and the variability of sperm morphology among iguanian lizards. J Anat 204:451–464.

Wiens JJ. 2004. The role of morphological data in phylogeny reconstruction. Syst Biol 53:653–661.